Au@Ag Core–Shell Nanocubes with Finely Tuned and Well-Controlled Sizes, Shell Thicknesses, and Optical Properties

Yanyun Ma,[†,‡] Weiyang Li,[†] Eun Chul Cho,[†] Zhiyuan Li,[§] Taekyung Yu,[†] Jie Zeng,[†] Zhaoxiong Xie,[‡] and Younan Xia[†,*]

[†]Department of Biomedical Engineering, Washington University, St. Louis, Missouri 63130, United States, [‡]State Key Laboratory for Physical Chemistry of Solid Surfaces and Department of Chemistry, College of Chemistry and Chemical Engineering, Xiamen University, Xiamen, Fujian 361005, P. R. China, and [§]Institute of Physics, Chinese Academy of Sciences, Beijing 100080, P. R. China

ABSTRACT This paper describes a facile method for generating Au@Ag core–shell nanocubes with edge lengths controllable in the range of 13.4–50 nm. The synthesis involved the use of single-crystal, spherical Au nanocrystals of 11 nm in size as the seeds in an aqueous system, with ascorbic acid serving as the reductant and cetyltrimethylammonium chloride (CTAC) as the capping agent. The thickness of the Ag shells could be finely tuned from 1.2 to 20 nm by varying the ratio of $AgNO_3$ precursor to Au seeds. We also investigated the growth mechanism by examining the effects of seeds (capped by CTAC or cetyltrimethylammonium bromide(CTAB)) and capping agent (CTAC *vs* CTAB) on both size and shape of the resultant core–shell nanocrystals. Our results clearly indicate that CTAC worked much better than CTAB as a capping agent in both the syntheses of Au seeds and Au@Ag core–shell nanocubes. We further studied the localized surface plasmon resonance properties of the Au@Ag nanocubes as a function of the Ag shell thickness. By comparing with the extinction spectra obtained from theoretical calculations, we derived a critical value of *ca.* 3 nm for the shell thickness at which the plasmon excitation of the Au cores would be completely screened by the Ag shells. Moreover, these Au@Ag core–shell nanocubes could be converted into Au-based hollow nanostructures containing the original Au seeds in the interiors through a galvanic replacement reaction.

KEYWORDS: core–shell nanocubes · seed-mediated growth · cetyltrimethylammonium chloride · surface plasmonic property

Gold (Au) and silver (Ag) nanocrystals have received considerable attention for many years because of their fascinating optical properties known as localized surface plasmon resonance (LSPR),[1–4] and their widespread use in applications related to photonics, catalysis, information storage, chemical/biological sensing, and surface-enhanced Raman scattering (SERS).[5–10] In an effort to tailor their properties and thus improve their performance in various applications, people have developed a myriad of chemical methods for generating Au and Ag nanocrystals with a rich variety of shapes, including sphere, cube, decahedron, icosahedron, bipyramids, thin plate, rod, and wire.[11–20] Parallel to these developments, people have also looked into the possibility of combining Au and Ag into one single system to provide a new handle for controlling optical and catalytic properties. To this end, Au–Ag alloy and core–shell nanocrystals have been prepared and investigated in the context of catalysis, plasmonics, sensing, imaging, and biomedicine.[21–35] Particularly, by combining Au and Ag into a core–shell configuration, their LSPR properties can be potentially tailored and finely tuned by varying the size/shape of the core and the thickness of the shell as well as the coupling between the core and the shell.

For core–shell nanocrystals, it is relatively easy and straightforward to generate Au (or an alloy of Au and Ag) shells on Ag cores (*i.e.*, in the form of Ag@Au) because of a spontaneous galvanic replacement reaction between Ag nanocrystals and a salt precursor to elemental Au such as $AuCl_4^-$ or $AuCl_2^-$.[36] By controlling the volume of the salt precursor titrated into an aqueous suspension of Ag nanocrystals, one can readily control the thickness of the shells and thus the optical properties of the products. It might also be possible to directly generate Au coatings on Ag nanocrystals through the use of a salt precursor and a very strong reducing agent, although it would be hard to exclude the involvement of a galvanic replacement mechanism. In comparison, the core–shell nanocrystals with an inverted structure (*i.e.*, Au@Ag consisting of a Au core and a Ag shell) can only be prepared *via* the conformal coating of Ag on Au nanocrystals in a solution phase. In general, it should not be difficult to generate a conformal coating of Ag on the surface of an Au nanocrystal due to their close match of the lattice constant (the difference is only 0.2%) and thus the assurance of epitaxial growth. However, the deposited Ag can evolve into different shapes or

*Address correspondence to xia@biomed.wustl.edu.

Received for review September 1, 2010 and accepted October 14, 2010.

Published online October 22, 2010.
10.1021/nn102237c

morphologies depending on the experimental conditions such as the type of Au seeds (*e.g.*, the size, shape, facets, and capping agent), the precursor to elemental Ag, the reductant, the capping agent present in the reaction solution, the solvent, and the temperature. All of these variables make this seemingly simple process hard to control and worthy of systematic investigation.

To date, Au@Ag core−shell nanocrystals with various morphologies have been synthesized using an epitaxial growth process that involves conformal deposition of Ag on the surface of Au seeds.[21−32] For example, Fan *et al*. synthesized Au@Ag nanocubes by using 30-nm Au octahedra as seeds.[22] Tsuji *et al*. and Wang *et al*. demonstrated the seed-dependent evolution of shape for Au@Ag core−shell structures with various morphologies (decahedron, cube, rod, and octahedron, among others) by depositing Ag onto the surface of a mixture of Au nanocrystals with different shapes.[23−26] Pastoriza−Santos *et al*. and our group have reported the synthesis of Au@Ag core−shell octahedra using Au nanorods as seeds.[27,28] Mirkin *et al*. have synthesized Au@Ag core−shell nanoprisms by using Au nanoparticles (5 or 11 nm) or Au nanoprisms (~144 nm) as seeds.[29,30] However, in all of these studies, the Ag shell was not evenly deposited on the entire surface of the Au core because of the highly anisotropic shapes of Au seeds used in the syntheses. The shell thickness could vary significantly from place to place across the surface of an Au@Ag core−shell nanostructure. As a result, it has been very hard to derive the critical shell thickness at which the plasmon excitation of the Au cores would be completely screened by the Ag shells. It has also been difficult to resolve the correlation between the core−shell structures (*e.g.*, the shell thickness and overall edge length) and the corresponding LSPR properties.

Here we report a facile route to the synthesis of Au@Ag core−shell nanocubes with relatively high yield (86−90%) in an aqueous solution. The edge lengths of the cubes can be finely controlled from 13.4 to 50 nm by using single-crystal spherical Au nanocrystals (11 nm, cuboctahedron) as the seeds and cetyltrimethylammonium chloride (CTAC) as a capping agent to direct the growth of Ag shells. The thickness of the Ag shells can be precisely controlled in the range of 1.2 to 20 nm due to the spherical shape and high uniformity for the Au seeds. These Au@Ag nanocubes with highly tunable and controllable sizes and shell thicknesses allowed us to systematically investigate their LSPR properties and obtain, for the first time, the critical shell thickness at which the plasmon excitation of the core will be completely screened by the shell. It is also worth pointing out that it has been very difficult to obtain Ag nanocubes with edge lengths smaller than 25 nm when a hydrophilic system based on polyol reduction is used.[37] In a recent study, we obtained Ag nanocubes as small as 13.5 nm, but only with a hydrophobic system based on isoamyl ether.[38] In the present work, we demonstrate that the sizes of the Au@Ag cubes can be controlled as small as 13.4 nm by using 11-nm Au seeds.

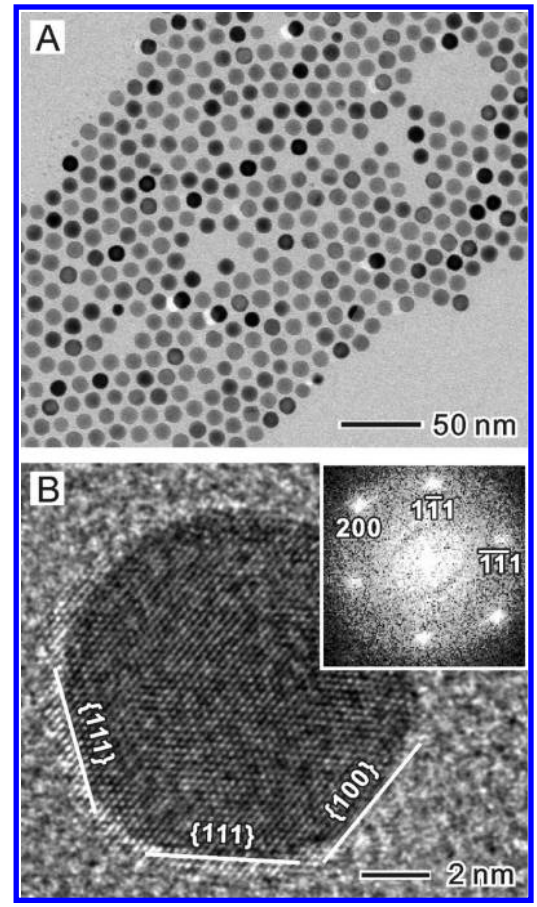

Figure 1. (A) TEM and (B) high-resolution TEM images of the Au nanocrystal seeds (11.0 ± 0.5 nm) prepared using a two-step procedure, with CTAC serving as the capping agent. The seed can be considered as a cuboctahedron enclosed by a mix of {100} and {111} facets.

RESULTS AND DISCUSSION

Synthesis of Au@Ag Core−Shell Nanocubes. We employed a seed-mediated growth process to prepare the Au@Ag Core−Shell nanocubes. The Au seeds were, in turn, synthesized using a two step procedure: (i) Very small (2−3 nm) Au nanocrystallites were synthesized by reducing $HAuCl_4$ with $NaBH_4$ in the presence of cetyltrimethylammonium bromide (CTAB), and (ii) these Au nanocrystallites were allowed to grow into Au nanocrystal seeds of 11 nm in size in the presence of additional $HAuCl_4$, ascorbic acid (AA), and CTAC. Figure 1A shows a typical transmission electron microscopy (TEM) image of the as-prepared Au nanocrystal seeds, which exhibited a spherical shape and were uniform in size (11 ± 0.8 nm). As indicated by the high-resolution TEM image (Figure 1B), these spherical seeds were single-crystal cubo-octahedrons (or truncated octahedrons) enclosed by a mix of {100} and {111} facets on the surface. In the following discussion, the Au nanocrystal seeds prepared using this specific procedure and capping agent are referred to as CTAC−Au seeds.

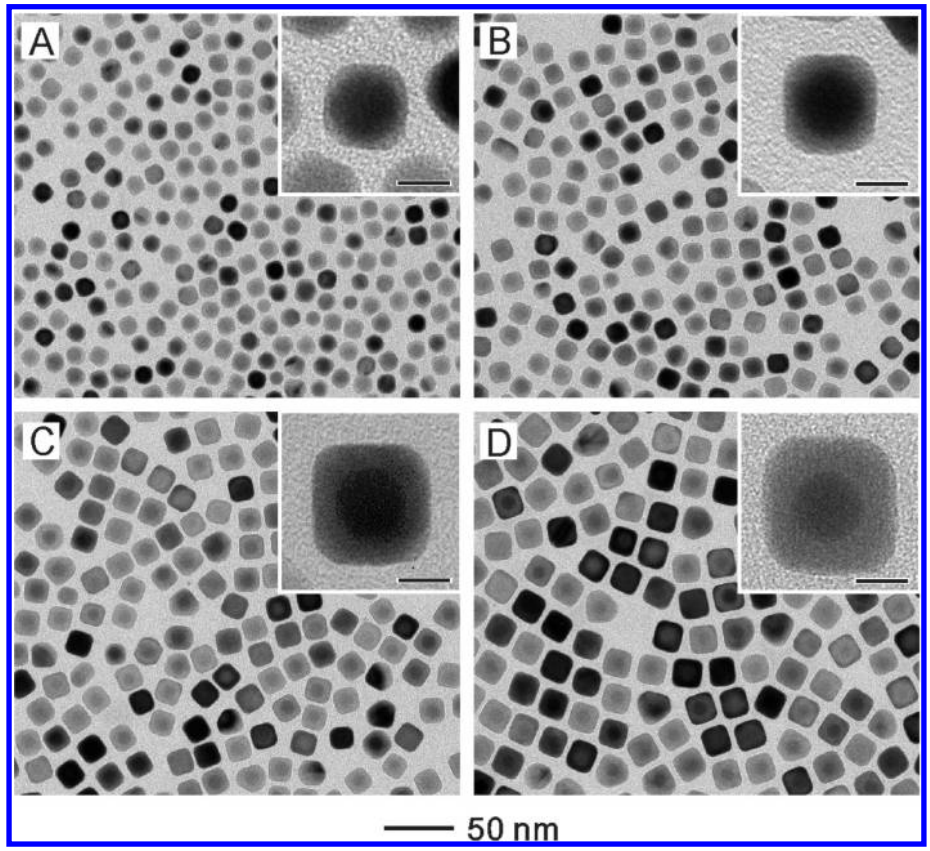

Figure 2. TEM images of Au@Ag core−shell nanocubes obtained by injecting different volumes of $AgNO_3$ (2 mM) into 5 mL solutions containing the same amount of Au seeds (14.6 mg/L) at 60 °C. The volumes of $AgNO_3$ were (A) 0.25 mL (edge length of the cubes, 13.4 ± 0.6 nm), (B) 0.5 mL (edge length of the cubes, 15.2 ± 0.6 nm), (C) 1 mL (edge length of the cubes, 17.2 ± 0.7 nm), and (D) 2 mL (edge length of the cubes, 20.0 ± 0.6 nm). After injection, the final concentrations of $AgNO_3$ were 0.09, 0.17, 0.29, and 0.44 mM, respectively. Insets are the corresponding high-magnification TEM images with the scale bars being 8 nm.

The Au@Ag core−shell nanocubes were formed by depositing Ag on the as-prepared CTAC−Au seeds. In a typical synthesis, we added $AgNO_3$ (the precursor to elemental Ag), AA (the reducing agent), and CTAC (the capping agent) into an aqueous suspension containing the Au seeds held at 60 °C. Cubic Au@Ag core−shell nanocrystals were formed due to the conformal overgrowth of Ag on the CTAC−Au seeds. As a major advantage of seed-mediated synthesis, the size of the resultant Au@Ag core−shell nanocrystals could be controlled from approximately 13 to 50 nm by varying either the amount of $AgNO_3$ or the amount of Au seeds added into the reaction solution. Figure 2 shows TEM images of the Au@Ag nanocubes obtained by injecting different volumes of $AgNO_3$ (2 mM) into aqueous suspensions containing the same amount of Au seeds. It can be seen that the edge lengths of the resultant Au@Ag cubes increased from 13.4 to 15.2, 17.2, and 20 nm when the volume of $AgNO_3$ solution was increased from 0.25 to 0.5, 1, and 2 mL. It is worth pointing out that these values were very close to the edge lengths (12.5, 14.5, 17.4, and 21.4 nm) calculated based on the number of Au seeds and the amount of $AgNO_3$ added. The inset in each image gives a magnified TEM image of the core−shell cubes. A clear difference in contrast can be observed between the Au core and the Ag shell due to the difference in atomic number and thus attenuation of electrons. It is clear that essentially every cube contained one Au nanocrystal seed in its center. The Ag shell was evenly deposited on the Au seeds, forming a complete coating on the Au core. As the surface of the Au@Ag nanocubes was dominated by the {100} facets,[25] we can deduce that the growth rate of Ag on the {111} facets of the Au seed was faster than the growth rate on the {100} facets. Otherwise, the deposited Ag should have evolved into octahedrons with a large fraction of {111} facets on the surface.

Figure 3 shows TEM images of the Au@Ag core−shell cubes obtained by injecting the same amount of $AgNO_3$ (5 mL, 2 mM) into aqueous suspensions containing different amounts of the Au seeds. The edge length of the cubes increased from 24.4 to 30.4, 42.6, and 50.4 nm when the concentration of the Au seeds was reduced from 14.6 to 7.3, 2.9, and 1.46 mg/L while the volume of the seeds was fixed at 5 mL. The Au core (in the center) and the Ag shell can also be easily distinguished from the TEM images at a higher magnification (see the insets).

Comparison of Different Capping Agents. It has been known that the choice of a capping agent can greatly

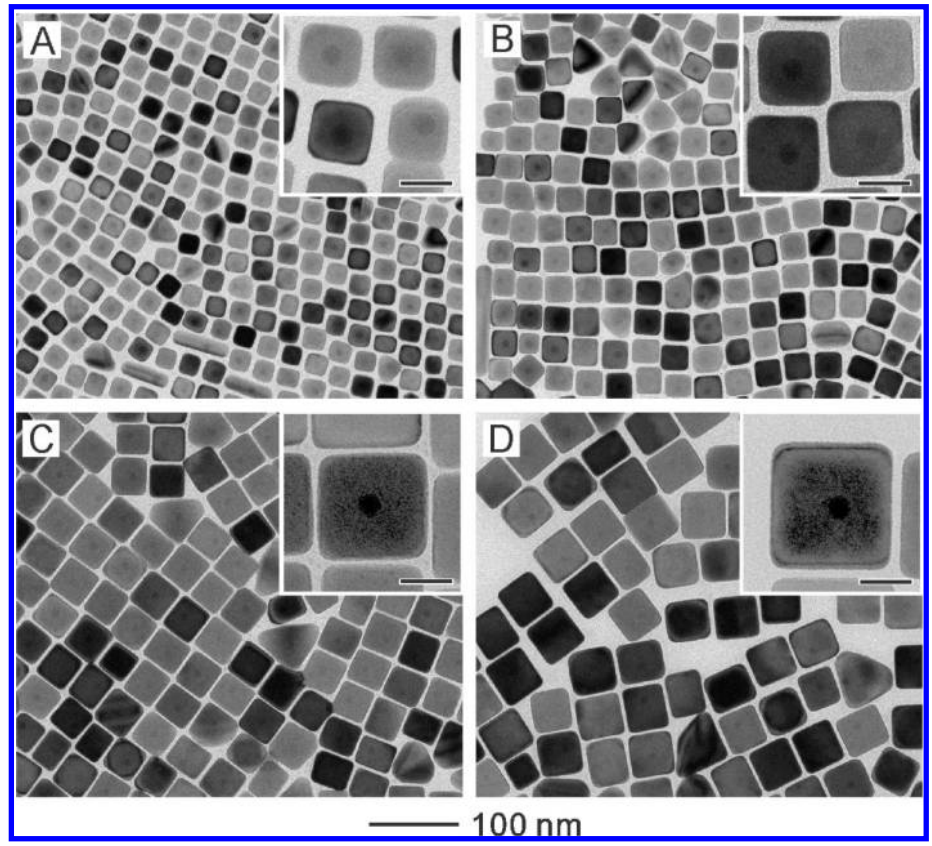

Figure 3. TEM images of Au@Ag core−shell nanocubes obtained by injecting 5 mL of $AgNO_3$ solution (2 mM) and 5 mL of AA solution (50 mM) into 5 mL of solutions with different seed concentrations: (A) 14.6 mg/L (edge length of the cubes, 24.4 ± 0.9 nm), (B) 7.3 mg/L (edge length of the cubes, 30.4 ± 1.2 nm), (C) 2.9 mg/L (edge length of the cubes, 42.6 ± 1.7 nm), (D) 1.46 mg/L (edge length of the cubes, 50.4 ± 2.2 nm). After injection, the final concentration of $AgNO_3$ was 0.67 mM. The reaction temperature was controlled at 60 °C. Insets are the corresponding high-magnification TEM images with the scale bars being 20 nm.

influence the final shape of the nanocrystals as well as their sizes.[14,39] Figure 4 shows TEM images of the samples prepared under the same condition as in Figure 2, except the use of CTAB instead of CTAC as a capping agent during the growth of Ag. In this case, the size of the cubes did not show significant change when the added volume of $AgNO_3$ solution was increased. Moreover, the samples obtained at a large amount of $AgNO_3$ exhibited poor uniformity in terms of both shape and size (Figure 4D). This result indicates that although CTAB can also direct Ag to grow to cubic nanocrystals on the Au seeds, this capping agent could not be used to control the size as we have achieved with CTAC. We also observed that when CTAB was used as a capping agent, the reaction solution turned from transparent to turbid as the volume of $AgNO_3$ was increased. This change could be ascribed to the formation of silver bromide (AgBr) from $AgNO_3$ (Ag^+) and CTAB (Br^-). When a large amount of $AgNO_3$ was added into the reaction solution, the AgBr became a precipitate due to its limited solubility in water. This is supported by the fact that the solubility of AgBr (described by the constant of a solubility equilibrium, $K_{sp} = 7.7 \times 10^{-13}$) is much lower than that of AgCl ($K_{sp} = 1.56 \times 10^{-10}$) at 25 °C.[40] As a result, even though a larger amount of $AgNO_3$ was applied, the concentration of Ag^+ available for the growth of Au@Ag cubes was rather limited due to the formation of a large quantity of water-insoluble AgBr, which was harder to be reduced than Ag^+ ions when AA was used as a reductant.

To better understand the influence of a capping agent on the synthesis of Au@Ag core−shell nanocrystals, we also prepared CTAB−Au seeds (see Figure S1 in the Supporting Information) by using a procedure similar to what was used to prepare the CTAC−Au seeds, except for the introduction of CTAB as a capping agent. As shown in Figure S1A, neither the size distribution (13.8 ± 1.2 nm) nor the shape of the CTAB−Au seeds was as uniform as the CTAC−Au seeds. The spherical nanoparticles were also found to be single-crystal, truncated octahedrons (Supporting Information, Figure S1B), similar to the CTAC−Au seeds. However, the sample also contained many triangular particles in addition to the spherical ones. Based on our previous studies, these triangular particles could be assigned to truncated bipyramids characterized by a singly twinned structure.[41] During the prepartion of Au seeds, oxidative etching played an important role in the formation of single-crystal Au seeds with high uniformity. The formation of such twinned structure could

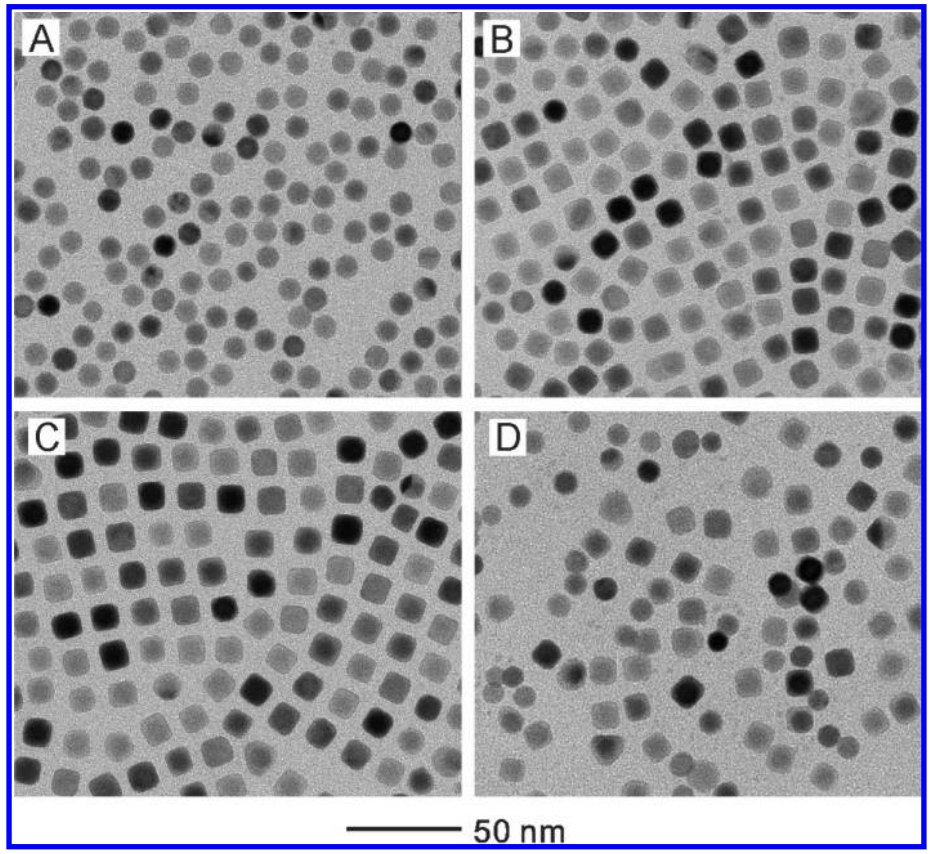

Figure 4. TEM images of the samples prepared under the same condition as in Figure 2, except the use of CTAB instead of CTAC as a capping agent during the growth of silver. After the injection of $AgNO_3$ and AA, the concentrations of $AgNO_3$ were: (A) 0.09, (B) 0.17, (C) 0.29, and (D) 0.67 mM, respectively.

be attributed to the weaker oxidative etching power for the Br^- in CTAB as compared to the Cl^- in CTAC because the chloride ions released by the Au precursor ($HAuCl_4$) are not sufficient to dissolve the twinned seeds of Au.[41]

We then tried to generate Au@Ag cubes by depositing Ag onto these CTAB−Au seeds. Supporting Information Figure S2 shows TEM images of the Au@Ag nanocubes prepared under the same condition as in Figure 2, except for the use of CTAB− rather than CTAC−Au seeds. It is clear that the size of the Au@Ag core−shell nanocubes could still be controlled from approximately 15 to 32 nm by varying the amount of $AgNO_3$ added into the reaction solution. However, the yield of the cubes (80−82%) was lower compared to those of samples prepared from the CTAC−Au seeds where the yields of cubes were typically in the range of 86−90%. Many bipyramid core−shell nanocrystals can be observed in the sample, which could have grown from the triangular particles found in the CTAB−Au seeds. Supporting Information Figure S3 shows TEM images of the samples prepared under the same condition as in Figure 4, except for the use of CTAB−Au seeds. A similar outcome was also observed in that we could not control the size when CTAB was used as a capping agent to grow Ag no matter what kind of seeds was used.

Figure 5 summarizes the effects of the two different capping agents on the outcomes of seed-mediated growth when two different types of Au seeds were used. When CTAC was used as the capping agent during growth, the size of the resultant Au@Ag cubes linearly increased with the volume (or final concentration)

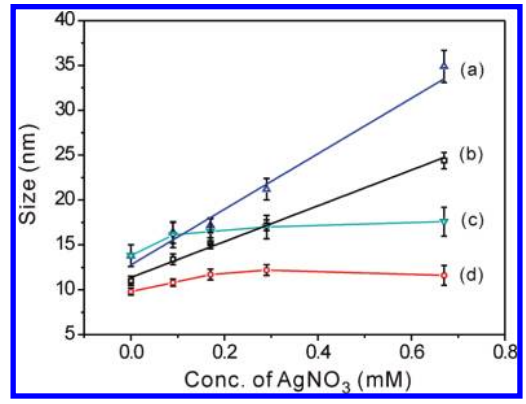

Figure 5. Plots summarizing the dependence of size on the concentration of $AgNO_3$ for the four syntheses involving two different types of capping agents for both Au seeds and Au@Ag cubes: (a, c) CTAB−Au seeds were used for the growth of silver in solutions containing (a) CTAC and (c) CTAB, respectively. (b, d) CTAC−Au seeds were used for the growth of silver in solutions containing (b) CTAC and (d) CTAB, respectively. The sizes refer to the edge length for the Au@Ag cubes, and the diameter for the spherical Au seeds, respectively.

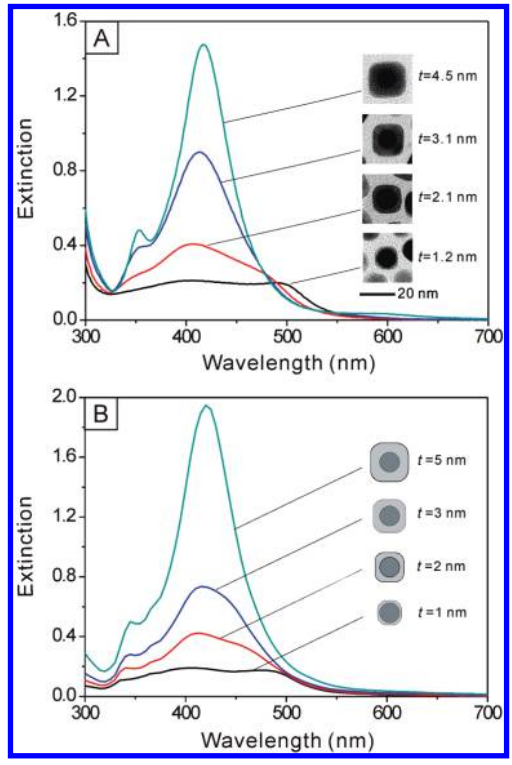

Figure 6. (A) UV−vis extinction spectra of Au@Ag core−shell nanocubes with different thicknesses (*t*) for the Ag shells. (B) Extinction spectra calculated for Au@Ag core−shell nanocubes with different shell thicknesses using the DDA method. We used a model with truncation at the corners and edges (see Supporting Information).

of Ag^+ solution regardless of the type of Au seeds used. In contrast, CTAB did not work well as a capping agent for the seeded growth in terms of size control over a broad range, primarily due to the formation of AgBr precipitate.

Optical Properties of the Au@Ag Core−Shell Nanocubes. The uniformity in shape as well as the ability to finely tune and control the thickness of Ag shells allowed us to systematically investigate the influence of shell thickness on the LSPR properties of the core−shell nanocrystals. Figure 6A shows UV−vis spectra taken from aqueous suspensions of Au@Ag core−shell cubes with different thicknesses (*t*) for the Ag shells (from 1.2 to 2.1, 3.1, and 4.5 nm), where the edge length of the nanocubes increased from 13.4 to 20 nm (see the Supporting Information for the definition of *t*). At a small *t* (1.2 nm), the Au@Ag nanocubes showed two characteristic peaks located at *ca.* 510 and 410 nm, representative of the Au core and the Ag shell, respectively. As expected, the intensity of peak for the Au nanocrystal seeds decreased as the thickness of the Ag shell increased. When the thickness of the shell increased to a critical point (t = 3.1 nm), the peak from the Au nanocrystal seeds disappeared, and only the peak for the Ag cubes remained. This result was consistent with the trend observed in theoretical calculations where the extinction spectra of Au@Ag core−shell nanocubes were computed using the discrete dipole approximation (DDA) method. The DDA calculation is able to provide both scattering and absorption spectra of nanoparticles with arbitrary shapes and with sizes on the order of, or less than, the wavelength of the incident light.[42] In the calculations, we assumed that the Au seeds were spherical with a diameter of 11 nm, and the average shell thickness of Ag was varied from 1 to 5 nm. We also considered the Ag nanocubes as being truncated at their corners and edges, similar to the Ag cubes obtained in our syntheses (see Supporting Information for a detailed description of the truncation in a model). As shown in Figure 6B, we also observed a trend for the change of LSPR peaks similar to the experimental observation, implying that the incident light could only penetrate Ag shells with a certain thickness around 3 nm. Beyond that, it will be impossible to excite the electrons in the Au cores. We also calculated the LSPR properties of the Au@Ag nanocrystals when the Ag shell took a spherical rather than a cubic shape by using Mie theory, which is suitable for any nanoparticle with a spherical shape.[42] The changes to the LSPR peaks (Supporting Information, Figure S4) were essentially the same as the results of experimental measurements and DDA calculations.

To confirm that the Au core and the Ag shell did not alloy during the synthesis, we monitored the changes to the extinction spectra by dissolving Ag from the as-prepared Au@Ag core−shell nanocubes (17.2 nm in edge length) with aqueous $Fe(NO_3)_3$ solution (0.05 M). It has been known that $Fe(NO_3)_3$ can be used as an etchant to dissolve Ag.[43] As shown in Supporting Information Figure S5A, the main LSPR peak shifted from around 410 nm (for Ag) to around 524 nm (for Au) when the volume of $Fe(NO_3)_3$ solution was increased from 0 to 0.08 mL. When 0.06 mL of the $Fe(NO_3)_3$ solution was added, the LSPR peak associated with the Ag shells completely disappeared, and only the peak for the Au cores remained. The TEM image (Supporting Information, Figure S5B) also clearly shows the existence of the Au cores obtained by dissolving Au@Ag core−shell nanocubes with 0.08 mL of $Fe(NO_3)_3$ solution.

When the edge length of the Au@Ag nanocubes was further increased beyond 20 nm, the LSPR spectra showed characteristic features of pure Ag nanocubes only. As shown in Figure 7A, the major LSPR peaks of the Ag nanocubes displayed a continuous red-shift along with the size increase. When the edge length of the cubes was increased from 24.4 to 30.4, 42.6, and 50.4 nm, the positions of the major LSPR peaks were shifted from 421 to 432, 454, and 466 nm, respectively. For the 42-and 50-nm samples, a split of LSPR peak around 390 nm appeared, indicating that the corners of the Ag nanocubes became sharper than those of the smaller nanocubes.[37] The small shoulder at ~530 nm could be due to the small amount (10−14%) of right bypramidal nanocrystals found in the sample.[13] The plot in Figure 7B suggests that there was a more or less linear

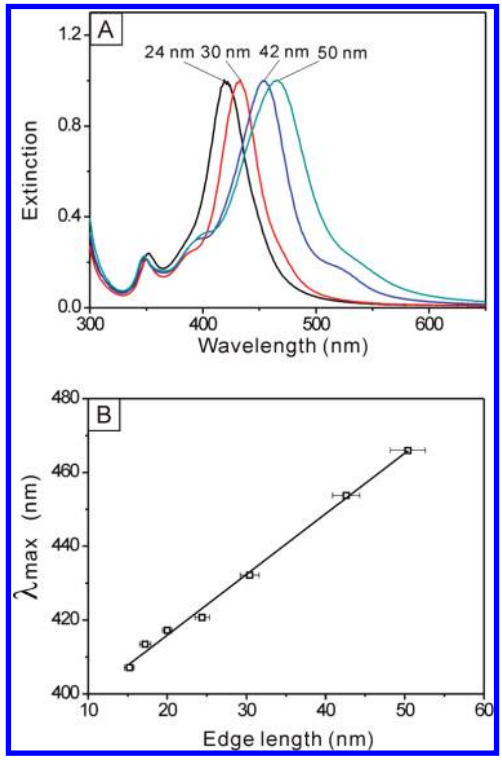

Figure 7. (A) UV−vis extinction spectra of Au@Ag core−shell nanocubes obtained under the same conditions shown in Figure 3, indicating that the main LSPR peak red-shifts with the increase in edge length. (B) A plot showing the linear dependence between the major LSPR peak position and the edge length for the Au@Ag core−shell nanocubes.

relationship between the LSPR peak position and the edge length of the Au@Ag nanocubes, which agrees with our previous observations with pure Ag nanocubes. The equation for describing the calibration curve was $\lambda_{max} = 1.66l + 383$ ($R^2 = 0.9947$), where λ_{max} and l are the peak position and edge length, respectively.

Synthesis of Au−Ag Hollow Nanostructures Containing Au Nanocrystals in the Interiors. One of the interesting features of the Au@Ag core−shell nanocubes is that the Ag shells can be transformed into porous shells of Au with slightly enlarged dimensions while the Au cores were kept inside the shells. The transformation can be easily achieved *via* a galvanic replacement process because the reduction potential of Ag is the lowest among the four noble metals (Pd, Pt, Au, and Ag).[27,32] In our previous study, we have demonstrated that Au, Pt, and Pd hollow nanostructures containing Au nanorods could be synthesized using a galvanic replacement reaction involving Au@Ag core−shell nanostructures derived from Au nanorods.[27] Here we shown that a similar approach can also be applied to the Au@Ag nanocubes with much smaller sizes (21 *vs* 50 nm). Figure 8, panels A and B show TEM images of two examples of such hollow nanostructures derived from Au@Ag nanocubes of 50 and 21 nm in edge length, respectively. The hollow nanostructures essentially retained their original cubic shape, and most of them contained the Au nanocrystal

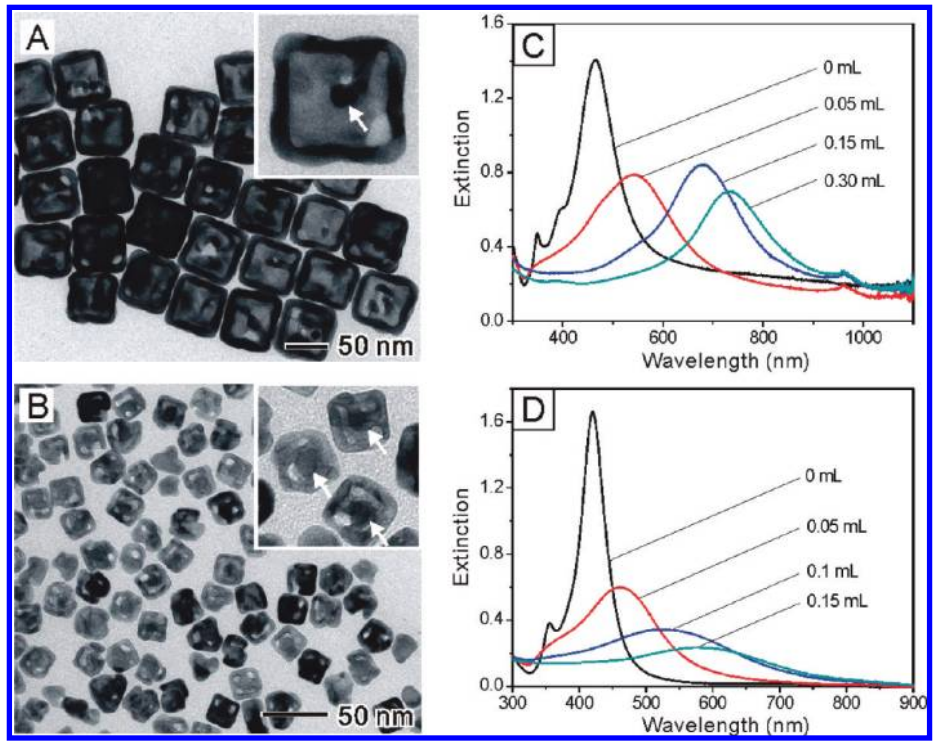

Figure 8. TEM images of Au-based nanocages derived from the Au@Ag nanocubes of (A) 50 and (B) 21 nm in edge length, respectively. The wall thicknesses of the Au nanocages were (A) 8.8 ± 0.9 and (B) 4.2 ± 0.4 nm, respectively. Insets show the corresponding images at higher magnification, clearly revealing the existence of the original Au seeds in the interiors (marked by white arrows). (C,D) UV−vis extinction spectra taken from aqueous suspensions of Ag nanocubes (C) 50 and (D) 21 nm, respectively, in edge length after they had been titrated with different volumes of an aqueous 0.5 mM $HAuCl_4$ solution (as labeled on each curve).

seeds, indicated by white arrows in the insets. The mechanism of this galvanic replacement reaction was discussed in detail in our previous work.[35]

Figure 8, panels C and D show UV−vis extinction spectra of the Au−Ag hollow nanostructures formed by adding different volumes of the 0.5 mM aqueous $HAuCl_4$ solution into the 50-nm and 21-nm Au@Ag nanocubes. It has been established that the LSPR properties of the Au−Ag nanostructures are determined by the ratio of outer edge length to wall thickness.[34−36] In principle, by controlling the volume of $HAuCl_4$, the LSPR peak positon could be continuously shifted toward longer wavelengths. In the present cases, the LSPR peak was continuously tuned from 450 to 750 nm for the 50-nm Au@Ag cubes, while it was only shifted from 410 to 600 nm for the 21-nm Au@Ag cubes. For hollow nanostructures with smaller size, it is more difficult to further reduce the wall thickness because the small hollow nanostructures tended to fragment into small pieces when more $HAuCl_4$ solution was added.

CONCLUSIONS

We have successfully demonstrated a facile approach to the preparation of Au@Ag core−shell nanocubes with relatively high yields (86−90%) *via* a water-based system, which is supposed to be environmentally friendlier than those involving organic solvents. The thickness of the Ag shell could be precisely tuned from 1.2 to 20 nm while the size of the cubes was increased from 13.4 nm to about 50 nm. Mechanistic studies showed that CTAC can act as an effective capping agent for both the preparation of Au seeds and the directed growth of the Ag shells. In comparison, CTAB was less effective in generating single-crystal Au seeds due to the weaker oxidative etching power relative to CTAC. CTAB was also not ideal for the growth step due to the formation of insoluble AgBr upon the addition of $AgNO_3$ solution. By systematically studying the LSPR properties of the Au@Ag core−shell nanocubes as a function of the Ag shell thickness, we obtained a critical value of 3 nm for the shell thickness at which the LSPR of the Au cores were completely screened by the Ag shells. Finally, we also demonstrated that these Au@Ag nanocubes could be converted into Au-based hollow nanostructures containing the Au seeds *via* a galvanic replacement reaction.

METHODS

Chemicals and Materials. Gold(III) chloride trihydrate ($HAuCl_4 \cdot 3H_2O$, ≥99.0%), silver nitrate ($AgNO_3$, >99%), sodium borohydride ($NaBH_4$, 99%), L-ascorbic acid (AA, >99%), poly(vinyl pyrrolidone) (PVP), cetyltrimethylammonium bromide (CTAB, ≥99%), and cetyltrimethylammonium chloride (CTAC, ≥98%) were all obtained from Sigma-Aldrich and used as received. In all experiments, we used deionized water with a resistivity of 18 MΩ, which was prepared using an ultrapure water system (Millipore).

Synthesis of Au Nanocrystal Seeds Capped with CTAC or CTAB. The Au nanocrystal seeds were prepared using a two-step procedure. We first made 3-nm Au nanoparticles by adding 0.6 mL of ice-cooled $NaBH_4$ solution (10 mM) into a 10 mL aqueous solution containing $HAuCl_4$ (0.25 mM) and CTAB (100 mM), generating a brownish solution. The seed solution was kept undisturbed for 3 h at 27 °C to ensure complete decomposition of $NaBH_4$ remaining in the solution.[42] For the synthesis of CTAC-capped Au seeds, 6 mL of aqueous $HAuCl_4$ solution (0.5 mM), 6 mL of aqueous CTAC solution (200 mM), and 4.5 mL of aqueous AA solution (100 mM) were mixed, followed by the addition of 0.3 mL of the 3-nm Au nanoparticles. The final mixture turned from colorless into red within 1 min, indicating the formation of larger Au nanocrystals. After 1 h, a UV−vis spectrum was recorded from the Au nanocrystal suspension and the products were collected by centrifugation (14 500 rpm, 30 min) and then washed with water once. After dispersing the nanocrystals in deionized water, the concentration of elemental gold in this seed solution was found to be 0.146 g/L (the corresponding number concentration of Au nanoparticles was 1.08×10^{16}/L) as determined by ICP−MS. For the synthesis of CTAB-capped Au seeds, the same method and addition sequence were used, except for the use of 6 mL of CTAB solution (200 mM) instead of CTAC solution in the growth of Au seeds. Also, the same washing conditions were used as for the CTAC-capped Au seeds.

Synthesis of Au@Ag Nanocubes with CTAC−Au Seeds in the Presence of CTAC. In a typical procedure, 0.5 mL of the CTAC−Au seeds and 4.5 mL of CTAC (20 mM) aqueous solution were mixed in a 20 mL vial. After the mixture was heated at 60 °C for 20 min under magnetic stirring, a specific volume of aqueous $AgNO_3$ solution (2 mM) and an aqueous solution of AA (50 mM) and CTAC (40 mM) were simultaneously injected at a rate of 0.2 mL/min using a syringe pump. The volume of AA (50 mM) added into the reaction solution was kept the same as that of $AgNO_3$. Different volumes (0.25, 0.5, 1, and 2 mL) of $AgNO_3$ were used to control the size of the resultant Au@Ag nanocubes from 13.4 nm up to 20 nm. After injection, the concentrations of $AgNO_3$ in the final solutions were 0.09, 0.17, 0.29, and 0.44 mM, respectively. During the injection, the reaction mixture turned from red to brownish-yellow. After 4 h, the vials were cooled in an ice-bath. The products were collected by centrifugation (14 500 rpm for 15 min) and then washed with water once.

To control the size of Au@Ag nanocubes in the range of 20−50 nm, we used different volumes (0.5, 0.25, 0.1, and 0.05 mL) of the CTAC−Au seeds. We kept the total volume of aqueous suspension containing the Au seeds and CTAC (20 mM) at 5 mL. After mixing the two aqueous solutions and heating them at 60 °C for 20 min under magnetic stirring, 5 mL of $AgNO_3$ (2 mM) aqueous solution and 5 mL of an aqueous solution containing AA (50 mM) and CTAC (40 mM) were simultaneously injected at a rate of 0.2 mL/min. Other procedures were the same as described above.

Synthesis of Au@Ag Nanocubes with CTAB−Au Seeds. The experiments were conducted in the same way as those with CTAC−Au seeds described in the previous sections, except for the use of different seeds.

Synthesis of Hollow Nanostructures Containing Au Nanocrystal Seeds. We prepared Au−Ag hollow nanostructures containing Au nanocrystal seeds *via* a galvanic replacement reaction between the Au@Ag nanocubes and aqueous $HAuCl_4$ solution. The Au@Ag nanocubes were collected by centrifugation (13 000 rpm for 15 min) and then redispersed in a solution of PVP (1 wt %) and CTAB (0.2 M) with a volume ratio of 1:1. Then, 1 mL of the Au@Ag nanocubes was heated at 90 °C for 2 min, followed by three additions of 0.5 mM $HAuCl_4$ solution. We recorded the UV−vis spectra as the volume of $HAuCl_4$ was increased to track the progress of the reaction. The hollow nanostructures were collected by centrifugation (13 000 rpm for 15 min) and washed with water twice.

Instrumentation. Transmission electron microscopy (TEM) images of the Au nanocrystals, Au@Ag nanocubes, and Au−Ag hollow nanostructures were obtained with a Technai G2 Spirit microscope operated at 120 kV (FEI, Hillsboro, OR). High-resolution TEM (HRTEM) images were obtained with a field-emission JEOL 2100F microscope operated at 200 kV (Tokyo, Japan). Extinction spectra of all the nanostructures were recorded using a UV−vis spectrometer (Varian, Cary 50). The concentration of gold was determined using an ICP−MS spectrometer (7500 CS, Agilent), which could be convert to the concentration of Au nanocrystals once the particle size had been measured by TEM imaging.

Acknowledgment. This work was supported in part by the NSF (DMR-0804088) and the NIH (1R01 CA138527). Y.X. was also partially supported by the World Class University (WCU) program through the National Research Foundation of Korea funded by the Ministry of Education, Science and Technology (R32-20031). As a jointly supervised student, Y.M. was also partially supported by a Fellowship from the China Scholarship Council. Part of the work was performed at the Nano Research Facility (NRF), a member of the National Nanotechnology Infrastructure Network (NNIN), which is supported by the NSF under Award No. ECS-0335765.

Supporting Information Available: TEM and high-resolution TEM images of CTAB−Au seeds, TEM images of the products prepared by CTAB−Au seeds, extinction spectra of Au@Ag nanospheres calculated using Mie theory, extinction spectra and TEM image of the products obtained by dissolving Au@Ag core−shell nanocubes with $Fe(NO_3)_3$ solution, definition of the thickness of Ag shells, and description of truncation in a model for Au@Ag nanocubes. This material is available free of charge *via* the Internet at http://pubs.acs.org.

REFERENCES AND NOTES

1. Murphy, C. J.; Sau, T. K.; Gole, A. M.; Orendorff, C. J.; Gao, J.; Gou, L.; Hunyadi, S. E.; Li, T. Anisotropic Metal Nanoparticles: Synthesis, Assembly, and Optical Applications. *J. Phys. Chem. B* **2005**, *109*, 13857–13870.
2. Zhang, J.; Liu, H.; Wang, Z.; Ming, N. Shape-Selective Synthesis of Gold Nanoparticles with Controlled Sizes, Shapes, and Plasmon Resonances. *Adv. Funct. Mater.* **2007**, *17*, 3295–3303.
3. Wiley, B. J.; Im, S. H.; Li, Z.; McLellan, J.; Siekkinen, A.; Xia, Y. Maneuvering the Surface Plasmon Resonance of Silver Nanostructures through Shape-Controlled Synthesis. *J. Phys. Chem. B* **2006**, *110*, 15666–15675.
4. Tao, A.; Sinsermsuksakul, P.; Yang, P. Polyhedral Silver Nanocrystals with Distinct Scattering Signatures. *Angew. Chem., Int. Ed.* **2006**, *45*, 4597–4601.
5. Pyayt, A. L.; Wiley, B.; Xia, Y.; Chen, A.; Dalton, L. Integration of Photonic and Silver Nanowire Plasmonic Waveguides. *Nat. Nanotechnol.* **2008**, *3*, 660–665.
6. Peng, S.; Lee, Y.; Wang, C.; Yin, H.; Dai, S.; Sun, S. A Facile Synthesis of Monodisperse Au Nanoparticles and Their Catalysis of CO Oxidation. *Nano Res.* **2008**, *1*, 229–234.
7. Murphy, C. J.; Gole, A. M.; Hunyadi, S. E.; Stone, J. W.; Sisco, P. N.; Alkilany, A.; Kinard, B. E.; Hankins, P. Chemical Sensing and Imaging with Metallic Nanorods. *Chem. Commun.* **2008**, 544–557.
8. Murphy, C. J.; Gole, A. M.; Stone, J. W.; Sisco, P. N.; Alkilany, A. M.; Goldsmith, E. C.; Baxter, S. C. Gold Nanoparticles in Biology: Beyond Toxicity to Cellular Imaging. *Acc. Chem. Res.* **2008**, *41*, 1721–1730.
9. Cao, Y. C.; Jin, R.; Mirkin, C. A. Nanoparticles with Raman Spectroscopic Fingerprints for DNA and RNA Detection. *Science* **2002**, *297*, 1536–1540.
10. Mulvihill, M. J.; Ling, X.; Henzie, J.; Yang, P. Anisotropic Etching of Silver Nanoparticles for Plasmonic Structures Capable of Single-Particle SERS. *J. Am. Chem. Soc.* **2010**, *132*, 268–274.
11. Wiley, B.; Sun, Y.; Mayers, B.; Xia, Y. Shape-Controlled Synthesis of Metal Nanostructures: The Case of Silver. *Chem.—Eur. J.* **2005**, *11*, 454–463.
12. Zheng, X.; Zhao, X.; Guo, D.; Tang, B.; Xu, S.; Zhao, B.; Xu, W. Photochemical Formation of Silver Nanodecahedra: Structural Selection by the Excitation Wavelength. *Langmuir* **2009**, *25*, 3802–3807.
13. Wiley, B. J.; Xiong, Y.; Li, Z.; Yin, Y.; Xia, Y. Right Bipyramids of Silver: A New Shape Derived from Single Twinned Seeds. *Nano Lett.* **2006**, *6*, 765–768.
14. Jin, R.; Cao, Y. C.; Hao, E.; Metraux, G. S.; Schatz, G. C.; Mirkin, C. A. Controlling Anisotropic Nanoparticle Growth through Plasmon Excitation. *Nature* **2003**, *425*, 487–490.
15. Niu, W.; Zheng, S.; Wang, D.; Liu, X.; Li, H.; Han, S.; Chen, J.; Tang, Z.; Xu, G. Selective Synthesis of Single-Crystalline Rhombic Dodecahedral, Octahedral, and Cubic Gold Nanocrystals. *J. Am. Chem. Soc.* **2009**, *131*, 697–703.
16. Seo, D.; Yoo, C. I.; Park, J. C.; Park, S. M.; Ryu, S; Song, H. Directed Surface Overgrowth and Morphology Control of Polyhedral Gold Nanocrystals. *Angew. Chem., Int. Ed.* **2008**, *47*, 763–767.
17. Sánchez-Iglesias, A.; Pastoriza-Santos, I.; Pérez-Juste, J.; Rodríguez-González, B.; García de Abajo, F. J.; Liz-Marzán, L. M. Synthesis and Optical Properties of Gold Nanodecahedra with Size Control. *Adv. Mater.* **2006**, *18*, 2529–2534.
18. Seo, D.; Yoo, C. I.; Chung, I. S.; Park, S. M.; Ryu, S.; Song, H. Shape Adjustment between Multiply Twinned and Single-Crystalline Polyhedral Gold Nanocrystals: Decahedra, Icosahedra, and Truncated Tetrahedra. *J. Phys. Chem. C* **2008**, *112*, 2469–2475.
19. Yavuz, M. S.; Li, W.; Xia, Y. Facile Synthesis of Gold Icosahedra in an Aqueous Solution by Reacting $HAuCl_4$ with *N*-Vinyl Pyrrolidone. *Chem.—Eur. J.* **2009**, *15*, 13181–13187.
20. Millstone, J. E.; Métraux, G. S.; Mirkin, C. A. Controlling the Edge Length of Gold Nanoprisms *via* a Seed-Mediated Approach. *Adv. Funct. Mater.* **2006**, *16*, 1209–1214.
21. Gonzalez, C. M.; Liu, Y.; Scaiano, J. C. Photochemical Strategies for the Facile Synthesis of Gold−Silver Alloy and Core−Shell Bimetallic Nanoparticles. *J. Phys. Chem. C* **2009**, *113*, 11861–11867.
22. Fan, F.; Liu, D.; Wu, Y.; Duan, S.; Xie, Z.; Jiang, Z.; Tian, Z. Epitaxial Growth of Heterogeneous Metal Nanocrystals: From Gold Nano-octahedra to Palladium and Silver Nanocubes. *J. Am. Chem. Soc.* **2008**, *130*, 6949–6951.
23. Wu, Y.; Jiang, P.; Jiang, M.; Wang, T.; Guo, C.; Xie, S.; Wang, Z. The Shape Evolution of Gold Seeds and Gold@Silver Core−Shell Nanostructures. *Nanotechnology* **2009**, *20*, 305602.
24. Tsuji, M.; Maeda, Y.; Hikino, S.; Kumagae, H.; Matsunaga, M.; Tang, X.; Matsuo, R.; Ogino, M.; Jiang, P. Shape Evolution of Octahedral and Triangular Platelike Silver Nanocrystals from Cubic and Right Bipyramidal Seeds in DMF. *Cryst. Growth Des.* **2009**, *9*, 4700–4705.
25. Tsuji, M.; Miyamae, N.; Lim, S.; Kimura, K.; Zhang, X.; Hikino, S.; Nishio, M. Crystal Structures and Growth Mechanisms of Au@Ag Core−Shell Nanoparticles Prepared by the Microwave-Polyol Method. *Cryst. Growth Des.* **2006**, *6*, 1801–1807.
26. Tsuji, M.; Matsuo, R.; Jiang, P.; Miyamae, N.; Ueyama, D.; Nishio, M.; Hikino, S.; Kumagae, H.; Kamarudin, K. S. N.; Tang, X. Shape-Dependent Evolution of Au@Ag Core−Shell Nanocrystals by PVP-Assisted *N,N*-Dimethylformamide Reduction. *Cryst. Growth Des.* **2008**, *8*, 2528–2536.
27. Cho, E. C.; Camargo, P. H. C.; Xia, Y. Synthesis and Characterization of Noble-Metal Nanostructures Containing Gold Nanorods in the Center. *Adv. Mater.* **2010**, *22*, 744–748.
28. Sanchez-Iglesias, A.; Carbo-Argibay, E.; Glaria, A.; Rodriguez-Gonzalez, B.; Perez-Juste, J.; Pastoriza-Santos, I.; Liz-Marzan, L. M. Rapid Epitaxial Growth of Ag on Au Nanoparticles: From Au Nanorods to Core-Shell Au@Ag Octahedrons. *Chem.—Eur. J.* **2010**, *16*, 5558–5563.
29. Xue, C.; Millstone, J. E.; Li, S.; Mirkin, C. A. Plasmon-Driven Synthesis of Triangular Core−Shell Nanoprisms from Gold Seeds. *Angew. Chem., Int. Ed.* **2007**, *46*, 8436–8439.

30. Yoo, H.; Millstone, J. E.; Li, S.; Jang, J.; Wei, W.; Wu, J.; Schatz, G. C.; Mirkin, C. A. Core−Shell Triangular Bifrustums. *Nano Lett.* **2009**, *9*, 3038–3041.
31. Liu, M.; Guyot-Sionnest, P. Synthesis and Optical Characterization of Au/Ag Core/Shell Nanorods. *J. Phys. Chem. B* **2004**, *108*, 5882–5888.
32. Seo, D.; Song, H. Asymmetric Hollow Nanorod Formation through a Partial Galvanic Replacement Reaction. *J. Am. Chem. Soc.* **2009**, *131*, 18210–18211.
33. Hu, K. W.; Liu, T. M.; Chung, K. Y.; Huang, K. S.; Hsieh, C. T.; Sun, C. K.; Yeh, C. S. Efficient Near-IR Hyperthermia and Intense Nonlinear Optical Imaging Contrast on the Gold Nanorod-in-Shell Nanostructures. *J. Am. Chem. Soc.* **2009**, *131*, 14186–14187.
34. Hunyadi, S. E.; Murphy, C. J. Bimetallic Silver-Gold Nanowires: Fabrication and Use in Surface-Enhanced Raman Scattering. *J. Mater. Chem.* **2006**, *16*, 3929–3935.
35. Chen, J.; Wiley, B.; Li, Z.; Campbell, D.; Saeki, F.; Cang, H.; Au, L.; Lee, J.; Li, X. ; Xia, Y. Gold Nanocages: Engineering Their Structure for Biomedical Applications. *Adv. Mater.* **2005**, *17*, 2255–2261.
36. Au, L.; Lu, X.; Xia, Y. A Comparative Study of Galvanic Replacement Reactions Involving Ag Nanocubes and $AuCl_2^-$ or $AuCl_4^-$. *Adv. Mater.* **2008**, *20*, 2517–2522.
37. Siekkinen, A. R.; McLellan, J. M.; Chen, J.; Xia, Y. Rapid Synthesis of Small Silver Nanocubes by Mediating Polyol Reduction with a Trace Amount of Sodium Sulfide or Sodium Hydrosulfide. *Chem. Phys. Lett.* **2006**, *432*, 491–496.
38. Ma, Y.; Li, W.; Zeng, J; McKiernan, M.; Xie, Z.; Xia, Y. Synthesis of Small Silver Nanocubes in A Hydrophobic Solvent by Introducing Oxidative Etching with Fe(III) Species. *J. Mater. Chem.* **2010**, *20*, 3586–3589.
39. Zeng, J.; Zheng, Y.; Rycenga, M.; Tao, J.; Li, Z.; Zhang, Q.; Zhu, Y.; Xia, Y. Controlling the Shapes of Silver Nanocrystals with Different Capping Agents. *J. Am. Chem. Soc.* **2010**, *132*, 8552–8553.
40. Adamson, A. W. *Textbook of Physical Chemistry,* 3rd ed.; Academic Press: Orlando, FL, 1986; pp 473.
41. Li, W.; Xia, Y. Facile Synthesis of Gold Octahedra by Direct Reduction of $HAuCl_4$ in an Aqueous Solution. *Chem. Asian J.* **2010**, *5*, 1312–1316.
42. Kelly, K. L.; Coronado, E.; Zhao, L.; Schatz, G. C. The Optical Properties of Metal Nanoparticles: The Influence of Size, Shape, and Dielectric Environment. *J. Phys. Chem. B* **2003**, *107*, 668–677.
43. Li, W.; Camargo, P. H. C.; Au, L.; Zhang, Q.; Rycenga, M.; Xia, Y. Etching and Dimerization: A Simple and Versatile Route to Dimers of Silver Nanospheres with a Range of Sizes. *Angew. Chem., Int. Ed.* **2010**, *49*, 164–168.